

## Mechanism of Zonal Index Evolution in a Two-Layer Model

SUKYOUNG LEE

*Department of Meteorology, The Pennsylvania State University, University Park, Pennsylvania*

STEVEN FELDSTEIN

*Earth System Science Center, The Pennsylvania State University, University Park, Pennsylvania*

(Manuscript received 3 July 1995, in final form 8 February 1996)

### ABSTRACT

A mechanism that drives a zonal jet to meander in the meridional direction is investigated with a two-layer multiwave quasigeostrophic  $\beta$ -plane channel model. This model isolates the zonal index characteristics of a purely eddy-driven jet. Empirical orthogonal function analysis is used to characterize the northward- and southward-shifted states of the jet, and the authors refer to these two states as "high" and "low" zonal indexes, respectively. Composite analysis is used to examine the evolution of the zonal-mean flow, eddy heat and momentum fluxes, storm tracks, and energetics associated with both zonal indexes. It is found that the zonal index is the most prominent form of variability over a broad range of meridional scales for the initially unstable region.

As expected, the onset of either index is marked by an anomalous momentum flux convergence–divergence pair on either side of the time-mean jet, and the high and low indexes are dynamically equivalent. This eddy forcing of the zonal-mean flow takes place on a timescale much shorter than that for the persistence of the zonal index itself. During most of the zonal index persistence, the zonal wind anomaly decays slowly. From a qualitative viewpoint, the zonal index can be interpreted as being impulsively forced by the eddies. Both the composite analysis and maps of instantaneous potential vorticity suggest that the zonal index persistence is not maintained by eddy–zonal-mean flow feedback. It is shown that the eddy forcing in normal-mode baroclinic life cycles does not explain the onset to either zonal index; however, its role during the zonal index persistence is inconclusive. When two consecutive persistent zonal index states are of opposite sign, the onset for the latter state is typically characterized by merging of two disturbances along two potential vorticity "fronts."

### 1. Introduction

Throughout the past two decades, there has been a great deal of interest in the low-frequency variability of the zonally asymmetric large-scale atmospheric circulation. More recently, attention has also been drawn toward the low-frequency variability of the zonally averaged flow. This research on low-frequency zonally averaged flow variability has included the use of both primitive equation models (Robinson 1991; Yu and Hartmann 1993) and observational studies of the Southern Hemisphere (SH) (Trenberth 1979; Kidson 1988; Karoly 1990; Nigam 1990). Historically, low-frequency variability of the zonally averaged flow was examined from the viewpoint of the zonal index, a quantity first introduced by Rossby (1939), which he defined as the difference between the zonally averaged sea level pressure between 35°N and 55°N. At that time, it was hoped that the zonal index could aid in forecasting the longitudinal position of the ultralong plan-

etary waves. Furthermore, Willett (1948) noted that the zonal index is associated with latitudinal shifts of the westerly jet. In the present paper, we refer to the zonal index as the meridional meander of the zonally symmetric westerly jet and define the high (low) index as a state where the latitudinal position of the jet is displaced northward (southward) of the time-mean jet.

The mechanism for excitation of the zonal index was discussed in Trenberth (1984), Karoly (1990), Robinson (1991), and Yu and Hartmann (1993). These authors all argue that either phase of the zonal index is driven by transient eddy-momentum flux convergence. Consider the following standard form for the quasigeostrophic (QG) zonal-mean, zonal momentum equation on a  $\beta$  plane that adequately describes large-scale mid-latitude motions:

$$\frac{\partial \bar{u}}{\partial t} = f_0 \bar{v} - \frac{\partial (\overline{u'v'})}{\partial y} + \text{friction}, \quad (1)$$

where the overbar denotes a zonal mean and the prime indicates a deviation from the zonal mean. If (1) is vertically integrated over the depth of the fluid with standard boundary conditions (i.e., the vertical velocity vanishing at the lower boundary, density approaching

*Corresponding author address:* Dr. Sukyoung Lee, Department of Meteorology, The Pennsylvania State University, 503 Walker Bldg., University Park, PA 16802-5013.

zero at the top of the fluid, and the meridional velocity equaling zero at the channel wall) and if friction is negligible, then there is only one term on the rhs of (1) that can accelerate the zonal wind: the eddy momentum flux convergence.

Given the above arguments, however, it is still unclear how the anomalous momentum flux convergence comes about. For example, is it the barotropic decay stage of a normal-mode baroclinic life cycle, as suggested by Yu and Hartmann (1993)? Or, is it associated with barotropic decay of a baroclinic wave that did not originate as a normal mode? It is also conceivable that the momentum flux convergence can occur in a random manner without any clear relationship to a baroclinic wave that grows and decays. Yet another possibility involves barotropic instability because a wave that grows due to barotropic instability can simultaneously destroy a jet on which it grows and establish a new jet elsewhere. Clearly, the first three mechanisms can account for the onset, persistence, and decay of the zonal index. On the other hand, the barotropic instability mechanism can only explain the transition between zonal indexes.

The primary purpose of this paper is to investigate the mechanisms of the onset, persistence, and decay of both zonal indexes. These are objectively defined in section 2b. In all of the previous modeling studies of the zonal index, a westerly jet on spherical geometry was examined. In the atmosphere or in models with earthlike parameters on the sphere, two distinct zonally averaged jets are rarely observed if the flow is averaged over a time period longer than a season. In the observations, a distinctly separate subtropical jet and eddy-driven midlatitude jet are observed during the SH winter over Australia. In the spherical models used by Robinson (1991) and Yu and Hartmann (1993), there is only one maximum time-mean jet, and therefore a clear distinction between the subtropical and the eddy-driven jet is impossible. When a jet has mixed characteristics that include both a subtropical and an eddy-driven jet, it is possible that not only eddy momentum flux divergence but also a Hadley cell, which converts absolute to relative angular momentum in its upper branch, can play a central role in determining the zonal-index characteristics (S. B. Feldstein and S. Lee 1996).

If the dynamics involved in the subtropical jet are not crucial for the zonal index, as implied by Robinson (1991) and Yu and Hartmann (1993), the fundamental mechanisms responsible for the zonal index must operate in a simple model, such as an eddy-driven, meridionally meandering jet on a  $\beta$  plane. Furthermore, if the eddies that force the zonal jet are synoptic-scale baroclinic waves, the essential mechanism for the zonal index should be captured within a quasigeostrophic framework. Therefore, in this study, we will use a two-layer quasigeostrophic  $\beta$ -plane model.

The premise of using this model also comes from the quasigeostrophic turbulence calculations of Panetta and Held (1988) and Panetta (1993). In these studies, multiple jets are spontaneously generated in both quasilinear (Panetta and Held 1988) and nonlinear models (Panetta 1993) without any "radiative relaxation forcing" toward an equilibrated jet structure, clearly demonstrating that these jets are eddy driven. Over a wide parameter space, these multiple jets also meander meridionally. It then seems reasonable to assume that these meandering, multiple jets are relevant for the zonal index. However, there is no reason to expect that these multiple jets and associated waves, or "storm tracks," are evolving independently of each other. In order to avoid possible complications that can arise from mutually interacting multiple jets, throughout most of this study we will examine the meridionally meandering jets in a parameter space where only one prominent jet can exist.

This paper is organized as follows. The model and analysis method are described in section 2. In section 3, we then examine in detail results from nonlinear model integrations. In section 4, we will explore the range of parameter space that allows for zonal index behavior and discuss the sensitivity to the zonal wave-number truncation. Concluding remarks follow in section 5.

## 2. Description of a model and analysis method

### a. A two-layer quasigeostrophic model

The dimensionless equations for the two-layer quasigeostrophic (QG) model on a  $\beta$  plane are

$$\frac{\partial Q_j}{\partial t} + J(\psi_j, Q_j) = -(-1)^j r \left( \frac{\psi_1 - \psi_2}{2} - \tau_e \right) - \delta_{j,2} \kappa_M \nabla^2 \psi_2 - \nu \nabla^6 \psi_j, \quad (2)$$

where

$$Q_j = \beta y + \nabla^2 \psi_j + (-1)^j \left( \frac{\psi_1 - \psi_2}{2} \right), \quad j = 1, 2, \quad (3)$$

and  $j = 1$  and  $2$  refer to the upper and lower layers, respectively. The velocity field is determined by the relation  $(u_j, v_j) = (-\partial\psi_j/\partial y, \partial\psi_j/\partial x)$ . The horizontal length scale is the radius of deformation  $\lambda$ . Time is nondimensionalized by  $\lambda/U_0$ , where  $U_0$  is the horizontal velocity scale. For convenience, in this study, we refer to one nondimensional time unit,  $\lambda/U_0$ , as one "day." The Ekman damping coefficient  $\kappa_M$  is included in the lower layer only. The additional parameters are  $r$  (strength of radiative damping),  $\nu$  (biharmonic diffusivity), and  $\beta$  (gradient of the Coriolis parameter). The values of  $\kappa_M$ ,  $r$ ,  $\nu$ , and  $\beta$  are fixed at  $0.1 \text{ days}^{-1}$ ,  $30^{-1} \text{ days}^{-1}$ ,  $6 \times 10^{-3}$ , and  $0.2$ , respectively.

We use the following form for the initial zonal-mean, zonal wind profile to balance the "radiative equilibrium temperature" field  $\tau_e(y)$ :

$$U_e = -2\partial\tau_e/\partial y$$

$$= \begin{cases} U_0 & |y - W/2| < W_c \\ U_0 \exp[-(y - W/2)^2/\sigma^2] & |y - W/2| > W_c. \end{cases} \quad (4)$$

This zonal wind field is constant in the center of the domain and exponentially decays to zero outside of this central region. The same zonal wind profile was used in Panetta and Held (1988). If  $W_c$  is zero, this wind profile simply becomes a Gaussian jet. We fix the value of  $\sigma$  at 4, but the width  $W_c$  will be varied.

As described in section 4, zonal index behavior is the dominant form of zonal flow variability over the parameter range  $1 \leq W_c < 13$ . In most of the analyses presented in this study, we fix  $W_c = 7$ , which falls in the middle of this parameter range.

The model is finite differenced in the meridional direction and is spectral in the zonal direction. The channel width  $W$  is fixed at 90, where the walls are located at  $y = 0$  and  $y = W$ . There are 300 grid points between the channel walls unless otherwise stated.

Two different versions of the model are used in this study; one is a "full" model that includes 20 zonal wavenumbers,  $k = 0.1, 0.2, \dots, 2.0$ , corresponding to a channel length of  $20\pi$ , and the other is a sector model that includes a fundamental zonal wavenumber of  $k = 0.5$  and three higher harmonics. This sector model is found to be useful for better understanding the zonal-index evolution.

For further description of this model, readers are referred to Lee and Held (1991) and references therein.

### b. Model output analysis and procedure

In this study, we define the zonal index as the principal component (PC) of the empirical orthogonal function (EOF) of the vertically averaged zonal-mean zonal wind  $U_b = (U_1 + U_2)/2$ , with the following meridional structure: a meridional dipole with its node located at the center of the time-mean jet. Similar definitions were used to define the zonal index in Kidson (1988) and Yu and Hartmann (1993). This structure for the EOF corresponds to meridional meander of the jet. As stated above, this is the first EOF over a broad range of values for the parameter  $W_c$ .

In order to examine the temporal evolution of the zonal index, we first define an episode of persistence based on the satisfaction of two conditions, the first involving pattern correlations (Horel 1985; Mo 1986) and the second dealing with the amplitude of the zonal index itself. The pattern correlation is

$$\rho(t, \tau) = \frac{\langle u'_b(y, t)u'_b(y, t + \tau) \rangle}{\mu[u'_b(y, t)]\mu[u'_b(y, t + \tau)]}, \quad (5)$$

where  $u_b$  represents deviation of  $U_b$  from the time mean,  $u'_b = u_b(y, t) - \langle u_b(y, t) \rangle$ , and  $\mu^2[u'_b(y, t)] = \langle [u'_b(y, t)]^2 \rangle$ . The angle brackets denote a meridional average across the channel.

An episode of time is defined as being persistent if  $\rho(t, \tau)$  and  $\rho(t + 1, \tau)$  are both greater than a threshold value,  $\rho_c$ , for  $\tau = 1$  to 5 and if the magnitude of the zonal index is greater than one standard deviation. The threshold value  $\rho_c$  is chosen to correspond to the 95% significance level for a one-sided  $t$  test. The number of degrees of freedom for this test are obtained from the Fisher Z transformation. The onset day is defined as the first day of the persistent episode. However, in order to make sure that the amplitude of the zonal index is close to one standard deviation at the onset day, the onset day is shifted backward to the first day after which the magnitude of the zonal index exceeds one standard deviation. For further description of this analysis the reader is referred to S. B. Feldstein and S. Lee.

In this paper, composite analyses, based on the onset day as defined above, are extensively used to investigate the flow evolution associated with persistent zonal index episodes. However, it needs to be noted that compositing based on the onset day can artificially emphasize both the abruptness of the onset event and the slow decay of the anomaly. This is particularly important for red-noise processes that have no preferred timescale. Therefore, we performed a selection of composite calculations based on the middle day of the persistent episode. It was found that timescale associated with the onset of the zonal index anomaly was only slightly greater than that obtained with the composites based on the onset day. The timescale of the decay was essentially unaltered.

Each onset event is grouped into one of two categories; if two consecutive persistent episodes are of the same (opposite) sign, the onset to the former (latter) persistent episode is referred to as minor (major) onset. As we will see, the main difference between the two types of onset is that both the eddy fluxes and zonal-wind anomalies are greater for the major onset. In addition, by separating onset events into the two categories, different types of zonal index evolution can be identified.

## 3. Results

### a. A full model

In this section, we describe results from an 8500-day integration of the full model. The first 500 days are discarded, and the remaining 8000 days are analyzed. For the purpose of this study, it is important to analyze a time series that is long enough so that many low-frequency events can be sampled. On the other hand, because of the amount of available hard disk space, there is a limitation as to how often the model output

can be saved. It turns out, for the purpose of analysis, that it is sufficient to sample the model output every other day. This is because both the zonal-mean zonal winds and the transient eddy fluxes typically vary with a timescale longer than a few days.

The time-mean, zonal-mean zonal winds in the two layers and  $U_e$  are shown in Fig. 1. Although the zonal flow is relaxed back to the  $W_c = 7$  flat-top profile, the time-mean zonal flow exhibits a sharp jet structure in the middle of the channel. Figure 2 shows an example of a latitude-time segment for  $U_b$  during a 1000-day period of the model integration. Only the middle one-third of the channel,  $30 \leq y \leq 60$ , is shown. This figure clearly illustrates the strong tendency for latitudinal movement of the jet. This behavior is well captured in the first EOF (EOF1) of  $U_b$  (shown later in Fig. 13b). EOF1 explains 43.9% of the total variance. The power spectrum of the PC of EOF1 (not shown) follows that of a red-noise spectrum based on a lag 2-day autocorrelation, except for the presence of a statistically significant peak above the 99% level at 300 days. A similar power spectrum is obtained by Robinson and Qin (1992) in their zonal index study, except that their statistically significant peak occurs at 100 days (note that this cannot be directly compared with our result because a day in this study is defined as  $\lambda/U_0$ ). At present, we do not have a clear understanding of the physical mechanisms responsible for this spectral peak.

In this study, we will examine composites of several quantities for both the high and low indexes. However, it is important to note that the flow evolution for the low index is almost a mirror image of that for the high index. In fact, because there is no dynamical asym-

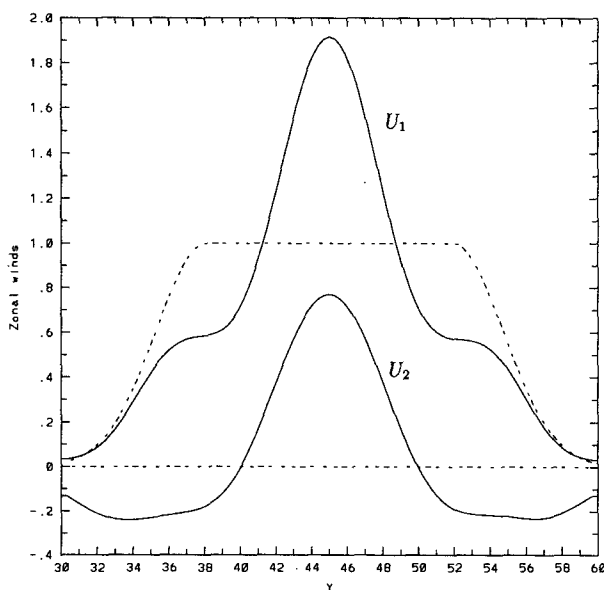


FIG. 1. Time-averaged zonal-mean winds from the full model calculation. The dashed line is the "radiative equilibrium" state  $U_e$ .

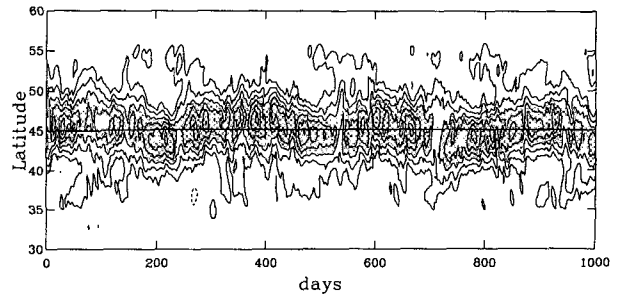


FIG. 2. Latitude-time segment of the barotropic zonal wind  $U_b$ . Solid contours are positive, dashed contours negative, and the zero contour is omitted. Contour interval is 0.3. Shading denotes values greater than or equal to 1.

metry about the center of the channel in this model, in the absence of sampling error, we expect precise antisymmetry between the high and low indexes. Therefore, in order to increase the sample size and to present our results in a concise manner, we will flip each composite for the high index about the center of the channel and then add it to the corresponding composite for the low index. In other words, composite structures will be shown only as low index cases, but the high index can be inferred by taking the mirror image.

Figure 3a shows the composite anomalous barotropic zonal wind for the major onset events. There are 37 major onset events that comprise this composite. Also shown next to Fig. 3a is the time-mean barotropic zonal wind, to be used as a reference for the anomalies. Consistent with our definition of major onset, there is a transition from high to low index that takes place at about 10 days before the onset day, and the maximum positive anomaly of the zonal wind appears shortly after lag zero ( $\tau = 0$ ) near  $y = 43$ . This zonal jet anomaly, however, is not maintained at a constant strength; instead, it slowly decays over an 80-day period. If we define persistence as the period during which the value of the PC for EOF1 remains above one standard deviation, the persistence lasts for 20 days. A qualitatively similar temporal evolution for the anomalous baroclinic winds, upper- and lower-layer potential vorticity (PV) gradient is also found (not shown), except that the latter quantity shows opposite sign.

Figures 3b and 3c show the vertically averaged eddy momentum flux convergence and eddy heat flux anomalies, respectively. Although not shown, during onset, the amplitude of the surface friction,  $\kappa_M \bar{U}_2$ , anomaly is much smaller than that of the vertically integrated eddy momentum flux convergence anomaly. As expected, because the eddies must force the persistent zonal-index event, there is maximum anomalous eddy momentum flux convergence at  $\tau = 0$ , with a positive center at  $y = 43$  and a negative center at  $y = 47$ . Comparing Figs. 3a,b, it is clear that the eddy forcing lasts for a very short time compared with the zonal wind anomaly

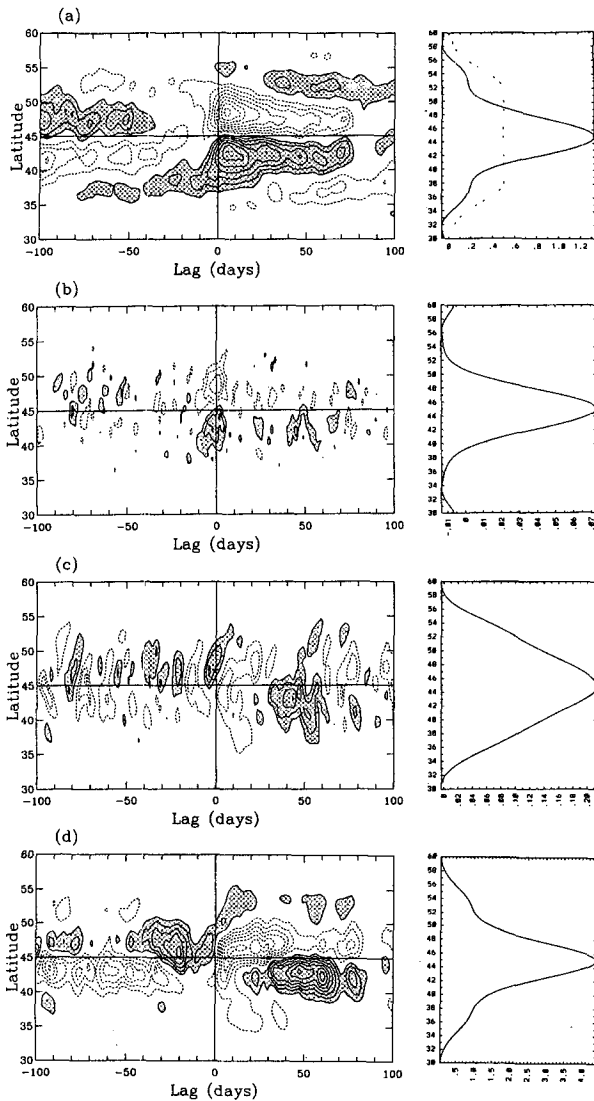


FIG. 3. Composites of the anomalous (a) barotropic zonal-mean zonal wind, (b) eddy momentum flux convergence, (c) eddy heat flux, and (d) upper-layer eddy streamfunction variance, relative to the major onset day (lag 0), from the full-model calculation. Solid contours are positive, dashed contours negative, and the zero contour is omitted. Contour intervals are (a) 0.05, (b) 0.015, (c) 0.015, and (d) 0.15. Shading denotes values greater than or equal to the smallest positive contour level. The right panel in each frame shows the corresponding time-mean value at each latitude.

itself. During onset, the largest positive heat flux anomaly occurs at  $\tau = -2$  days, mainly to the north of the channel center  $y_c$ . These results indicate that the anomalously strong momentum flux convergence is preceded by an enhanced heat flux. Furthermore, the relatively short timescale of the eddy momentum flux convergence (Fig. 3b) suggests that the eddy forcing of the zonal index is "impulsive" and that the persistence may be viewed as a slowly decaying state. Although a maximum heat flux anomaly occurs south of  $y_c$  for

$40 \leq \tau \leq 50$ , this local maximum does not accompany a significant degree of momentum flux convergence. In fact, by this time, the zonal wind anomaly has substantially weakened.

The temporal evolution of upper-layer streamfunction variance, or storm track, is shown in Fig. 3d. The sign of the anomaly pattern changes after the onset day. This indicates that the storm track anomaly lags the zonal wind anomaly, even though it is the storm track eddies that force the zonal wind to change prior to onset. Also, we note that for a period of 20 days following onset the storm track is weakened over a broad region. This behavior will be further discussed in section 3b in the context of wave breaking.

The composite energy budget based on either index is illustrated in Fig. 4. Consistent with the evolution of the eddy fluxes described above, during onset, the baroclinic energy conversion maximum precedes that for the barotropic energy conversion. However, the increase in the baroclinic growth is not as pronounced as that for the barotropic decay. Also, the eddy kinetic energy (EKE) does not have a distinctive maximum during the entire period shown in Fig. 4. This behavior is not difficult to understand because several waves with different structures can coexist simultaneously in a model with a full zonal wavenumber spectrum. Examples of such behavior can be seen in Figs. 5a and 5b, which show snapshots of the upper-layer PV during the onset for the high and low indexes, respectively. For the high index example (see Fig. 5a), although not every wave exhibits NE-SW tilting, there are two regions where the waves are clearly tilted with a NE-SW orientation. Similarly, in the low index example (see Fig. 5b), there is a localized wavy disturbance with distinctive NW-SE tilting.

The results from this low-resolution model calculation are compared with those from a version of the model with higher meridional resolution. In this version of the model, there are 900 grid points in the meridional direction, and the value of the biharmonic dif-

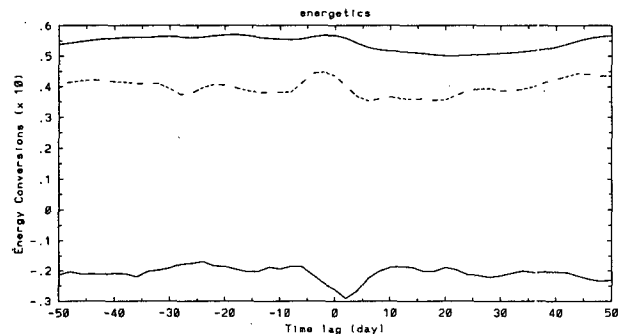


FIG. 4. Composite energetics relative to the major onset day from the full-model calculation. The curve with positive solid line is for eddy kinetic energy, dashed line for baroclinic energy conversion, and negative solid line for barotropic energy conversion.

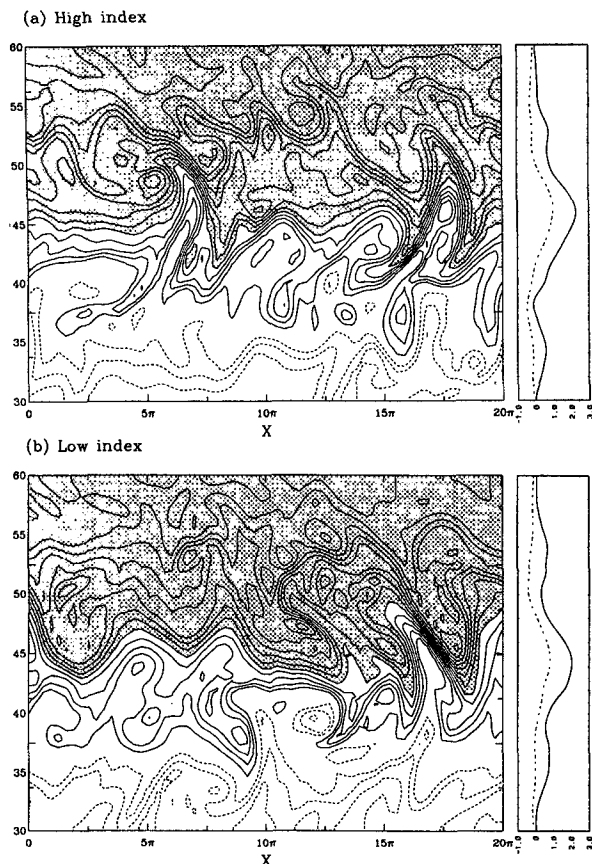


FIG. 5. Snapshots of upper-layer PV on the onset day for (a) the high index and (b) the low index, from the full model calculation. Contour interval is 1.0. The right panel in each frame shows the corresponding zonal-mean zonal wind for the upper layer (solid line) and lower layer (dashed line).

fusion coefficient is reduced to  $10^{-3}$ . All other model parameters remain unchanged. Due to the computational burden, this integration is only 2000 days long. It is found that the zonal index represents the dominant form of zonal-flow variability.

### b. A sector model

The previous section described the zonal index for the full model and showed that the eddy fluxes play important roles for the onset of the zonal index. Given that this full model can simulate zonal index behavior, we investigate whether the same behavior can be found in a corresponding sector model. If this is indeed the case, one can then use the concept of wave-mean flow interaction to better understand the evolution of the zonal index. For this purpose, we use a sector model where the fundamental zonal wavenumber  $k_0$  is chosen based on the full model calculation. Figure 6 shows the energy budget from the full model. The maximum eddy energy occurs at zonal wavenumber  $k = 0.5$ , and it is

this wavenumber that draws energy most efficiently from the zonal-mean flow (by efficient, it is meant that the energy conversion from the zonal mean to the eddies is largest for that zonal wavenumber), although the linearly most unstable zonal wavenumber of the initial flow is  $k = 0.7$ . Use of the most "efficient" wave in the study of wave mean flow interaction was discussed in the context of nonlinear baroclinic adjustment (Cai 1992; Chehelsky and Tung 1993). As we will shortly see, a sector model with fundamental zonal wavenumber  $k_0 = 0.5$  successfully captures the eddy fluxes and zonal-mean flow evolution found in the full model. However, the results from a sector model calculation with  $k_0 = 0.7$  are *qualitatively* different from those in the full model; with  $k_0 = 0.7$ , two distinct persistent zonal jets exist instead of one distinct, meridionally meandering zonal jet.

In addition to the fundamental zonal wavenumber  $k_0 = 0.5$ , there are three additional higher harmonics that will be retained in this sector model: these are  $k = 1.0$ , 1.5, and 2.0 in order to be consistent with the truncation of the full model. Aside from this truncation, the sector model is identical to the full model described earlier. This sector model is integrated for 8500 days, and the first 500 days are discarded. Once again, EOF analysis and sequences of statistically significant pattern correlations of  $u_b$  are used to define the onset and persistence of the zonal index. As with the results of the full model, the first EOF corresponds to the zonal index (see Fig. 7), explaining 46.8% of the total variance. This value for the variance of EOF1 is comparable to that in the full model. The power spectrum of the PC for EOF1 (not shown) is also very similar to that for the full model including the spectral peak at 300 days.

Figures 8a–d show composites of anomalous  $U_b$ , vertically averaged eddy momentum flux convergence, eddy heat flux, and storm tracks, respectively, based on

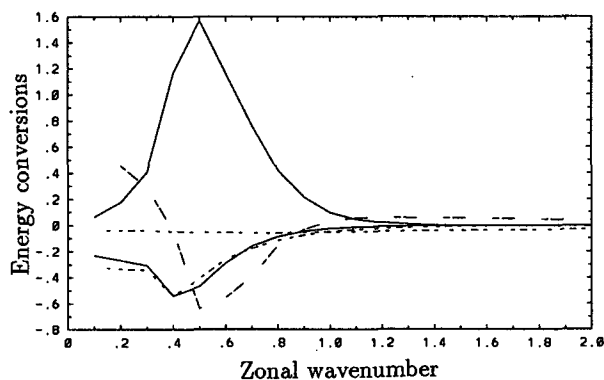


FIG. 6. Energy budget from the full-model calculation. The curve with positive solid line is the energy transfer from the zonal-mean flow to the eddies, negative solid line the energy loss due to radiative damping, negative short-dashed line the energy loss due to surface friction, long-dashed line the wave-wave energy transfer, and short-dashed line (close to zero) the energy loss due to diffusion.

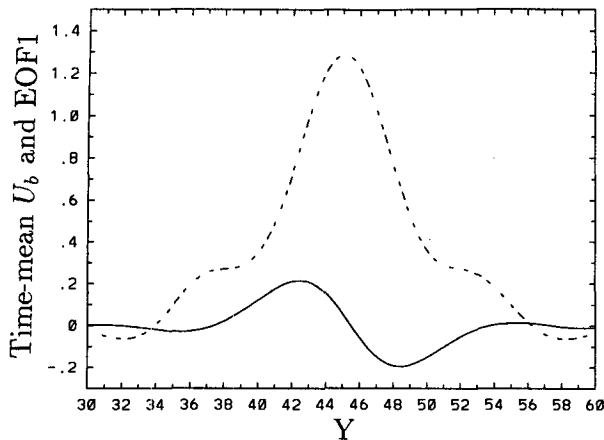


FIG. 7. EOF1 (solid line) and time-mean barotropic zonal wind (dashed line) from the sector model calculation.

the major onset. There are 47 major onset events that constitute these composites. Once again, because of antisymmetry, the high index composite is combined with the low index composite. Comparing Figs. 8a–d with Figs. 3a–d, the temporal evolution of both  $U_b$  and the eddy flux anomalies in the sector model are strikingly similar in their structure to those in the full model. The time-mean zonal winds and eddy fluxes are also shown in the right panels of Figs. 8a–d. Comparing Figs. 3a–d and Figs. 8a–d, the main similarities between the composites of the sector and full model results are 1) the dipole structure of the vertically averaged eddy momentum flux convergence during onset, 2) the heat flux maximum precedes that for the eddy momentum flux convergence–divergence pair, and 3) the persistence period is 20 days, which is much longer than the eddy forcing timescale. The main differences are 1) the amplitude of the anomalies are stronger in the sector model [perhaps this is not surprising, because wave–wave interaction can play a dissipative role (see Fig. 6)], and 2) away from the time of onset, the eddy fluxes are weaker in the sector model.

Figure 9 shows the composite EKE, baroclinic and barotropic eddy energy conversion based on the major onset. As for the full model, during onset, baroclinic growth is followed by barotropic decay. However, in contrast to the full model, the growth and decay of EKE, baroclinic growth, and barotropic decay are better defined. This is because there is only a single wave and its higher harmonics in this model so that the energetics of the wave that grows baroclinically and decays barotropically is not masked by other waves in the domain with different structures. The composite energetics in the sector model clearly indicate that the onset of a persistent zonal index is associated with a single episode of baroclinic growth followed by barotropic decay, consistent with the energetics of the full model. Also, the barotropic energy conversion is always neg-

ative, implying that barotropic instability is not operating during onset. Although energetics cannot confirm the presence of instability, they can indicate the absence of instability.

Figure 10 shows several snapshots of the upper-layer PV and the zonal-mean zonal winds in both layers before and after a typical major onset event for the low index. At  $\tau = -10$  days (Fig. 10a), there are two distinct PV “fronts”: one at the middle and the other on the northern side of the channel. At this time, these PV fronts exhibit no clear horizontal tilting. The maximum zonal wind is at  $y = 47$ , slightly poleward of the time-mean jet. These two PV fronts merge as they grow (see Fig. 10b), resulting in NW–SE tilting by the onset day (Fig. 10c) and a zonal wind increase (decrease) on the

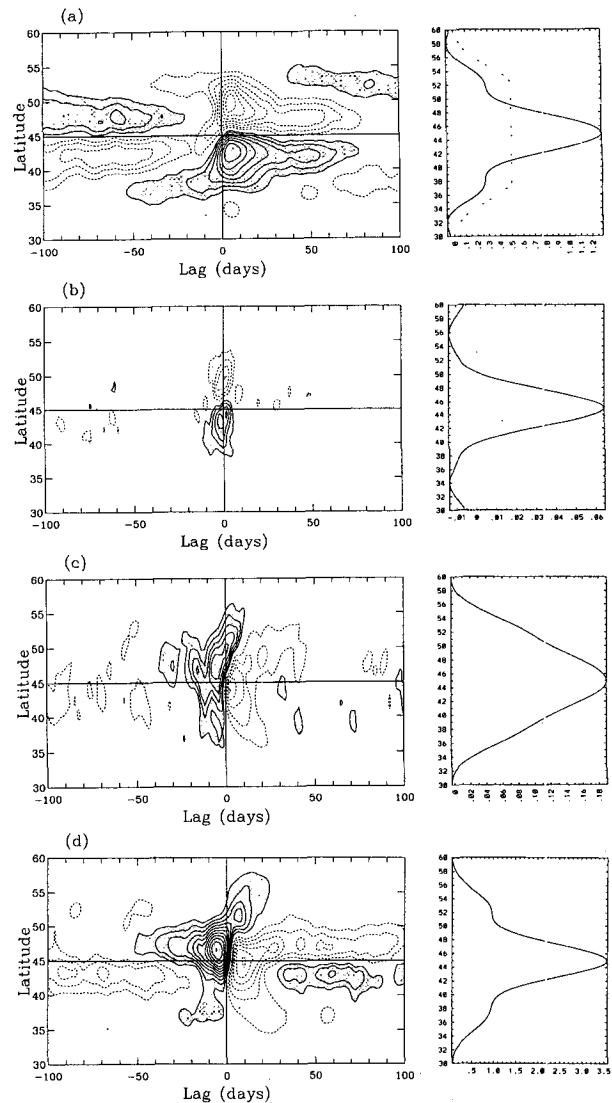


FIG. 8. As in Fig. 3 except from the sector model calculation. Contour intervals are (a) 0.1, (b) 0.03, (c) 0.03, and (d) 0.03.

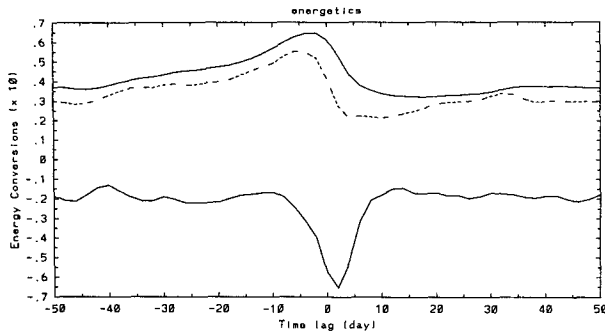


FIG. 9. As in Fig. 4 except from the sector model calculation.

southern (northern) side of the time-mean jet. As the NW–SE tilt increases, the wave starts to break, and the zonal winds on the southern side of  $y_c$  continue to increase. This process can be clearly seen at  $\tau = 4$  and 8 days, as shown in Figs. 10d and 10e, respectively. After the sharp tongue of low PV is ejected northward of the jet, mixing takes place in that region, and by  $\tau = 18$ , the flow on the southern side of the channel is left behind with a strong zonal flow and a small amplitude wave (Fig. 10f). This example illustrates that the persistence is characterized by a period of weak eddy amplitude after a wave breaking event. Furthermore, the above sequence of snapshots is consistent with the relatively brief eddy forcing followed by a period of suppressed storm track activity found in the composites (Figs. 8b and 8d). Although this example is typical for the major onset, there are some cases where a large amplitude wave develops shortly after the wave breaking. However, during the persistence phase, these large amplitude waves are typically not accompanied by a large momentum flux convergence and, thus, exert little influence on the zonal jet.

Figure 11 shows a composite of anomalous  $u_b$  based on the minor onset. This composite includes 76 minor onset events, almost twice as many as that for the major onset events. Results for minor onset are similar to those for major onset, including an average persistent period of 20 days, except that the maximum barotropic zonal wind anomaly appears less abruptly and is about 30% weaker (cf. Fig. 11 with Fig. 8a). The sign change in the zonal index occurs at  $\tau = -60$ , about 50 days earlier than the sign change for the major onset. For this reason, this composite is shown over a greater time period than that for the major onset composite. This extended growth period of the anomaly pattern leading up to onset is due to the occurrence of previous low-index events as specified by the definition of minor onset. The reason that this growth period does not include a secondary low index peak before onset is because the time interval between successive zonal index events of the same sign is highly variable. Also, consistent with the weaker zonal flow anomaly, the maximum eddy fluxes are weaker than those for the major

onset (not shown). For example, the maximum eddy momentum flux convergence is about 50% smaller for minor onset than that for major onset. Nevertheless, the qualitative structure of the eddy flux evolution is quite similar between major and minor onset, in particular the large-amplitude eddy forcing of the zonal-mean flow is confined to a period of several days.

### c. Baroclinic life cycle calculations

Because the energetics (Fig. 9) during onset are consistent with traditional baroclinic life cycle calculations (e.g., Simmons and Hoskins 1978; Feldstein and Held 1989), which exhibit baroclinic growth followed by barotropic decay, it is tempting to think that the zonal index is initiated by a normal-mode baroclinic life cycle, at least in the sector model. However, we argue that normal-mode instability and baroclinic life cycles associated with a single zonal wavenumber (and its higher harmonics) are unlikely to be relevant for both the onset and persistence of the zonal index for the following reasons. 1) During onset, the composite eddy heat flux (momentum flux convergence) is located on the northern (southern) side of  $y_c$ . Typically, during normal-mode baroclinic life cycles, the latitude of the two quantities approximately coincides [see Feldstein and Held (1989) and Fig. 7.5 in Hoskins (1983)]. 2) Major onset is often characterized by the merging of two PV fronts, which is not observed in normal-mode baroclinic life cycles. 3) Large amplitude disturbances are often present well before onset. 4) During persistence, the momentum flux convergence is negligible and the zonal-mean wind anomaly is decaying.

However, in light of the results of Yu and Hartmann (1993) that suggest baroclinic life cycles are responsible for maintaining the persistence phase, we carry out similar calculations using our experiments in order to further address the relevance of normal-mode baroclinic life cycles for the zonal index. In addition, with our sector model, self-consistent baroclinic life cycle calculations can be performed. This is because other zonal wavenumbers, whose role in the evolution of the flow is unclear, are absent in *both* the model integration and the life cycle calculations. In Yu and Hartmann (1993), nonlinear initial value experiments were performed using composite zonal winds for either phase of the zonal index as the initial state. However, it needs to be noted that their ‘‘nonlinear life cycle experiment’’ differs from the traditional life cycle calculations because diabatic forcing as well as frictional damping are included. Because such forcing and damping are not only operating on the wave component but also on the zonal-mean flow, the subsequent evolution of the flow can critically depend on the structure and amplitude of the initial perturbation. For example, if the projection of the initial disturbance onto the most unstable normal mode is weak and/or the amplitude of the initial disturbance is small, then the zonal-mean flow can be sig-

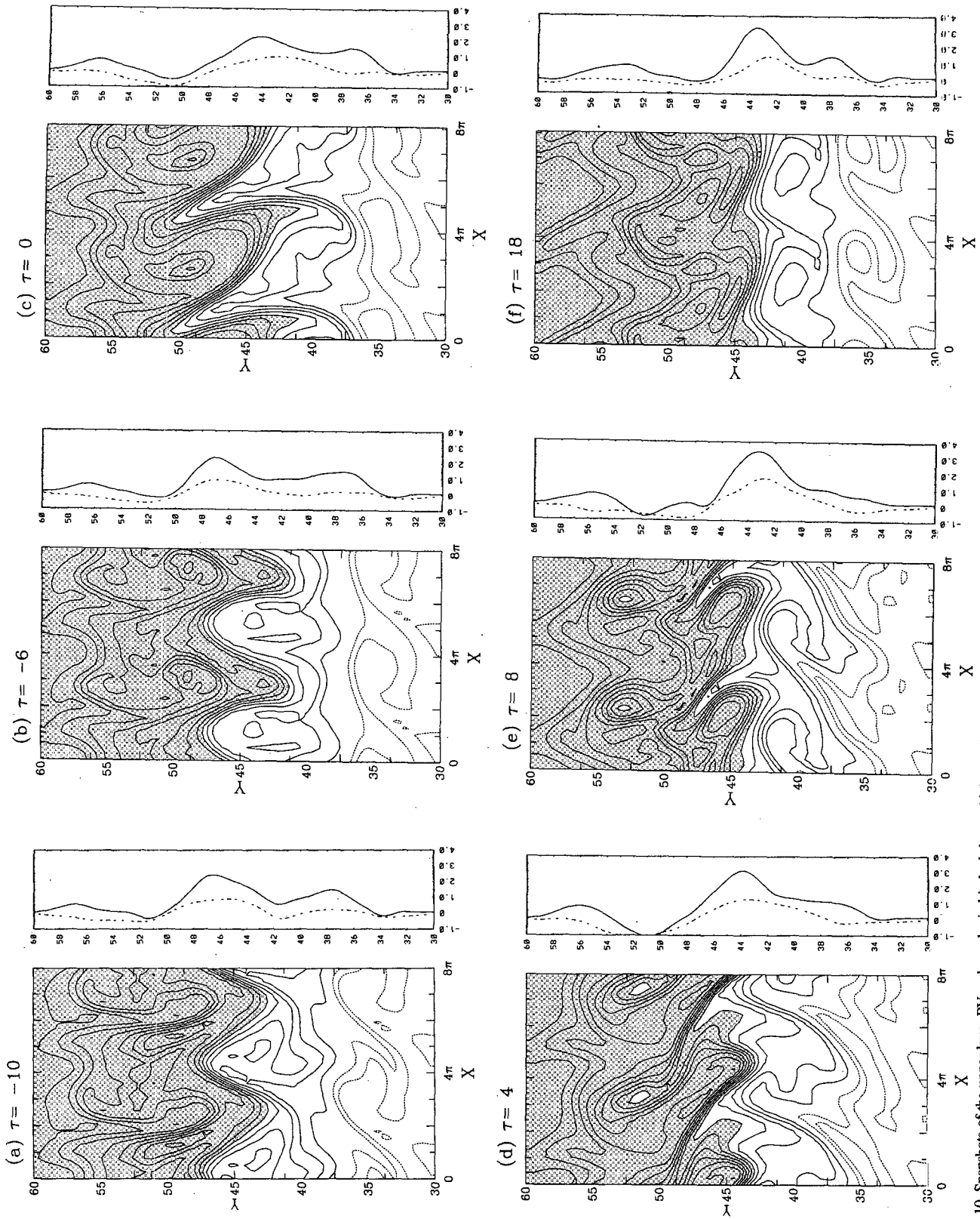


FIG. 10. Snapshots of the upper-layer PV and zonal wind in both layers (right panels) at  $\tau =$  (a)  $-10$ , (b)  $-6$ , (c)  $0$ , (d)  $4$ , (e)  $8$ , and (f)  $18$  days for a typical major onset event for the low index. These results are from the sector model calculation. Contour interval is  $1.0$ . The right panel in each frame shows the corresponding zonal-mean zonal wind for the upper layer (solid line) and lower layer (dashed line).

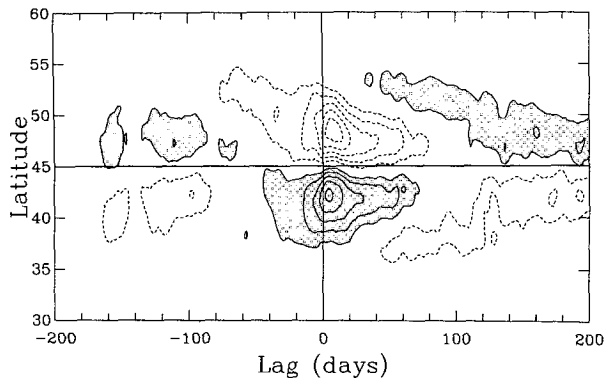


FIG. 11. Composite of anomalous barotropic zonal-mean zonal wind relative to the minor onset day from the sector model calculation. Solid contours are positive, dashed contours negative, and the zero contour is omitted. Contour interval is 0.1, and shading denotes values greater than 0.1.

nificantly altered by the forcing and damping before the disturbance can grow to large amplitude. As a result, a growing wave in such calculations may represent an unstable mode of an altered zonal-mean flow. Although we do not show the results, we performed many forced-dissipative life cycle calculations and found that not only the quantitative but also the qualitative structure of the growing disturbance is sensitive to its initial amplitude and structure. Given the ambiguity involved in the forced-dissipative life cycle calculations, in order to examine a clear relationship between the eddy and the zonal-mean flow, we decided to perform inviscid life cycle calculations.

The initial zonal-mean flow for the life cycle calculations is chosen from the composite flow at various  $\tau$ , in order to represent the flow prior to onset, at the time of onset, and during the persistence phase. A small amplitude, arbitrary disturbance is added to the zonal-mean flow, and this disturbance evolves toward the most unstable linear normal mode before its amplitude becomes large enough to alter the initial zonal-mean flow. The latitudinal acceleration and deceleration of the zonal-mean flow during the nonlinear decay stage corresponds very well with the structure of the momentum flux convergence of the most unstable normal mode. Figure 12 summarizes the results of the life cycle calculations, which shows the initial flow, momentum flux convergence of the most unstable normal mode, and the modified zonal-mean flow that follows immediately after the maximum barotropic energy conversion. All three quantities are vertically averaged. In that figure, the  $\tau$  corresponding to each frame is indicated by an arrow. Other calculations were also performed with initial zonal-mean winds corresponding to various  $\tau$  other than those indicated by the arrows. These calculations indicate that inside each of the following three time intervals the results are very similar:  $-20 \leq \tau \leq 4$ ,  $6 \leq \tau \leq 18$ ,  $20 \leq \tau \leq 46$ . From 20 days before

onset to 4 days after onset, both the eddy momentum flux convergence and the change in the zonal-mean wind occur north of  $y_c$ . This indicates that normal-mode instability and its nonlinear decay do not explain the onset for the low index. Due to dynamical symmetry, precisely the same statement can be made for the onset to the high index. After onset, that is, for  $\tau \geq 0$ , the structure and nonlinear evolution of the normal mode becomes more complex; for  $0 \leq \tau \leq 4$ , the zonal-mean flow acceleration occurs north of  $y_c$ , whereas for  $6 \leq \tau \leq 18$  the zonal wind acceleration occurs south of  $y_c$ . However, for  $20 \leq \tau \leq 46$ , the location of the zonal-mean flow acceleration moves back to the north of  $y_c$ . The above results show that the most unstable normal mode and corresponding nonlinear baroclinic life cycle can either maintain or terminate the persistence phase, which questions the notion that baroclinic life cycles can maintain either sign of the zonal index. Similar baroclinic life cycle experiments were performed for the minor onset composite. In this case, at all  $\tau$ , both before and after onset, the largest zonal-mean flow acceleration occurs north of  $y_c$ . This indicates that the fastest-growing normal mode and its life cycle cannot explain both onset and persistence.

Linear stability analysis based on the matrix eigenvalue approach was used to obtain a full set of unstable normal modes for  $-20 \leq \tau \leq 0$ . This analysis reveals that barotropic instability of the zonal-mean flow does not exist and therefore cannot account for the onset of either zonal index.

#### 4. Discussion

This section discusses additional results that are not described in section 3 yet provide useful insight into the zonal index phenomenon.

The temporal variability of the zonal flow is examined for different values of  $W_c$  [see (4)]:  $W_c = 0, 1, 3, 5, 9, 11, 13, 15$ , and 17, in addition to the  $W_c = 7$  case already examined in detail. As with the  $W_c = 7$  case, for each calculation, the full model is integrated for 8500 days and the last 8000 days are analyzed. For each of these cases, Table 1 lists the percentage of explained variance by the EOF associated with the zonal index, along with its corresponding ranking. Also, for selected cases among those listed above, Fig. 13 shows the time-mean barotropic zonal wind and the first EOF. For  $W_c = 0$ , the initial zonal wind profile is a Gaussian jet, with  $\sigma = 4$ . In this case, the most prominent mode of zonal-flow variability is strengthening and weakening of the jet, as shown in Fig. 13a; the zonal index corresponds to the third EOF in this case and explains only 18.3% of the total variance. However, for  $W_c = 1, 3, 5, 7, 9$ , and 11, the zonal index is the most prominent form of zonal-flow variability as it represents the largest fraction of the total variance. In each of these cases, the first EOF takes on a meridional dipole structure, as shown in Fig. 13b. As  $W_c$  is increased toward 13 and

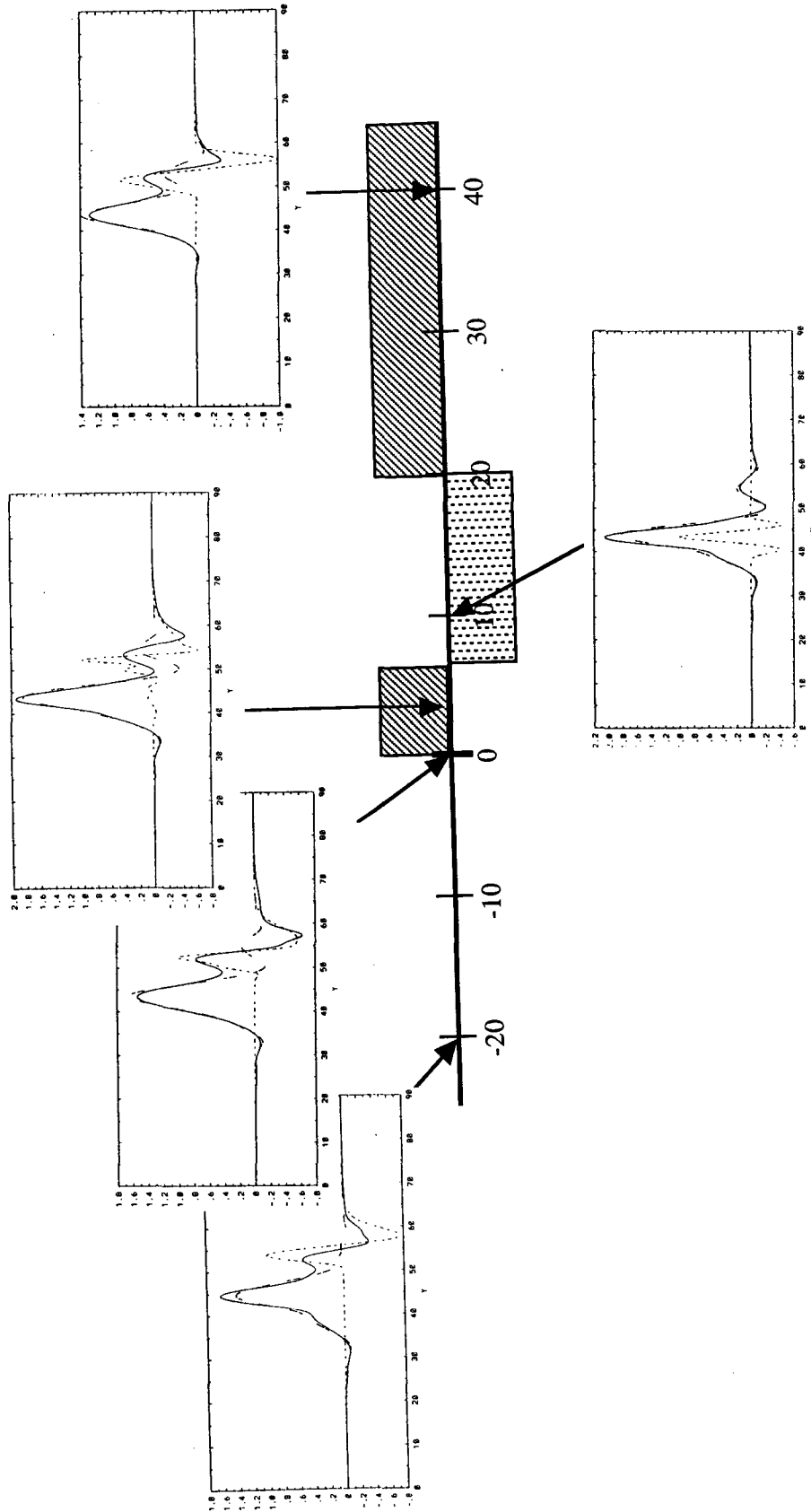


FIG. 12. Summary of baroclinic life cycle calculations. In each panel, long-dashed line is the initial zonal-mean zonal wind, the short-dashed line the eddy momentum flux convergence of the most unstable normal mode, and the solid line the modified zonal-mean zonal wind following the maximum barotropic energy conversion. All three quantities are vertically averaged, and the eddy momentum flux convergence is normalized by its maximum value. The arrow indicates the value of the lag  $\tau$  for which the composite zonal-mean zonal wind is used as the initial state. See text for more description.

TABLE 1. Percentage of explained variance by the EOF associated with the zonal index. The corresponding rank of the EOF is also indicated.

$W_c$	0	1	3	5	7	9	11	13	15	17
Variance (%)	18.3	38.6	56.7	45.3	43.9	40.4	35.5	27.4	18.9	32.3
Rank	3	1	1	1	1	1	1	2	2	1

15, the meridionally meandering, single prominent jet is no longer maintained at all times. Instead, the zonal flow is characterized by two alternating states, one being the familiar zonal index, with a single jet present, and the other being two prominent jets that undergo much less meridional meandering. The transition between these two states occurs over a relatively short time period, whereas each state can last several hundred days at a time. As a result, in these cases, it is found that the most dominant form of zonal flow variability is merging and splitting of the two jets (see Fig. 13c). For  $W_c = 17$ , two well-isolated jets appear at all times.<sup>1</sup> Interestingly, the dominant form of variability in this case is a simultaneous meridional displacement of the two jets (see Fig. 13d), which is equivalent to separate in-phase zonal-index behavior for each jet.

The above results suggest that the zonal index is most dominant over a wide range of parameter space, at least in this two-layer QG model. These results raise a fundamental question as to why the zonal index is such a prominent form of low-frequency zonal-flow variability. Given the fact that the zonal index is driven by the eddies, one can also view the zonal index as a phenomenon of meridionally meandering eddy activity. Therefore, if the role of the eddies is to remove the negative lower-layer meridional PV gradient  $\partial Q_2/\partial y$ , then one can think of the zonal index as a state in which the meridional size of the eddies is not large enough to fully remove the negative  $\partial Q_2/\partial y$  at a given time. If this is the case, the eddies must meander as they move to other regions of large negative  $\partial Q_2/\partial y$ . According to this picture, if the region of large negative  $\partial Q_2/\partial y$  can provide enough room for two meridionally aligned eddies, then two jets can coexist. This is consistent with the  $W_c = 17$  case. On the other hand, if the meridional scale of the eddies is comparable to that of the negative  $\partial Q_2/\partial y$  region, then one expects that zonal index behavior should be suppressed. For the  $W_c = 0$  case, where the zonal index accounts for only a small fraction of the total variance, the scale of the eddy and negative  $\partial Q_2/\partial y$  region are indeed found to be similar.

<sup>1</sup> We note that, if  $U_e$  takes the form of a Gaussian jet instead of the flat-top profile, this two-jet state does not persist even when the jet width is very large (e.g.,  $\sigma = 25$ ). Similar results are obtained in a simple two-layer model of the Antarctic Circumpolar Current by Treguier and Panetta (1994), in which two oceanic jets merge into one when meridional curvature is introduced into the surface wind stress profile.

If we are to extend the above arguments to a continuously stratified fluid, one may expect the eddies to meander meridionally, even when the scale of the eddies is comparable to the scale of the jet. This is because removal of the surface meridional temperature gradient  $\Delta\theta$  from one region must always result in an increase in  $\Delta\theta$  elsewhere. On the other hand, in the two-layer model, it is much easier for the eddies to homogenize the lower-layer zonal-mean PV field. This suggests that the insignificance of the zonal index for  $W_c = 0$ , as described earlier, might be an artifact of the two-layer model. Therefore, it may be that zonal index behavior is more prevalent in a continuously stratified flow.

Finally, we note that bimodal behavior of the zonal index is found for small values of  $\beta$  and  $\kappa_M$ , but only when a single zonal wavenumber is present in the model. Furthermore, this is the most unstable zonal wavenumber for the initial zonal flow, not the most energetic and/or efficient in a full model integration. In these experiments, the value of  $\sigma$  varies between 3

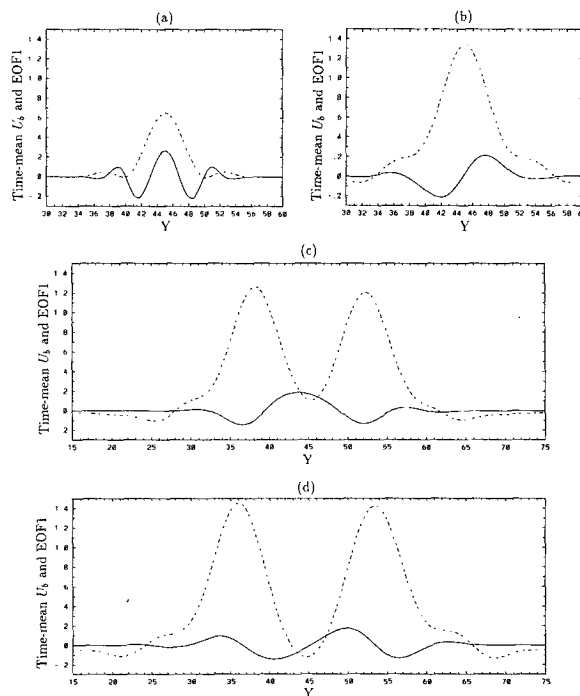


FIG. 13. EOF1 (solid line) and time-mean barotropic zonal wind (dashed line) for  $W_c =$  (a) 0, (b) 7, (c) 15, and (d) 17, from the full-model calculations.

and 5 and  $W_c$  is set to zero. These models exhibit bimodality in the sense that the zonal jet maximum persists either to the north or south of the initial jet for an unrealistically long period of time, for example, several thousand days. On the other hand, the transition from one index to another takes place within a few days, and the jet maximum never resides at the channel center. Because truncated models often exhibit bimodal behavior, this result may not be particularly surprising. However, this result suggests the need for caution when using a one-wave model for studying the zonal index.

## 5. Concluding remarks

This paper describes the evolution and mechanisms of meridionally meandering zonal jets in a two-layer QG model on a  $\beta$  plane. The meridional displacement of the zonal jet is objectively defined by the principal component of the EOF of the vertically averaged zonal wind that takes on a meridional dipole structure about the center of the time-mean jet. Unlike previous studies, the temporal evolution of the flow during onset and persistence of the zonal index is examined using composite analyses. Furthermore, in contrast to previous studies that do not distinguish between a subtropical and an eddy-driven jet, this channel model isolates zonal index characteristics of the eddy-driven jet. Due to the dynamical symmetry of this model about the center of the channel, the nature and mechanism of the zonal index are identical for either the high or low zonal indexes. Also, because the zonal-index evolution of the full model is quite well simulated by a sector model, the latter model is used extensively to understand the mechanisms behind the zonal index.

The main results of this study are as follows. 1) The timescale of the eddy forcing that initiates the zonal index is much shorter than that of the persistence phase. 2) The persistence of the zonal index is typically characterized by a period of slow decay of the anomalous zonal flow. During the persistence phase, the anomalous wave amplitude and eddy forcing tend to be small. The same behavior is found in S. B. Feldstein and S. Lee, which examined zonal index characteristics associated with the subtropical jet in an aquaplanet GCM. However, in that study, the onset to the high (low) zonal index is initiated by enhanced (weakened) eddy forcing. This contrasts with the results of the present study where both indexes are preceded by amplified eddy forcing. 3) The anomalous storm track follows the positive zonal-wind anomaly associated with the zonal index. For example, during the onset to the low index, the maximum storm track anomaly moves from the northern to the southern side of the time-mean jet. However, for a period of 20 days after onset, the storm track is temporarily weakened over the entire jet. This is consistent with the findings summarized above. 4) The zonal index is the most prominent form of zonal-flow variability over a wide

range of widths for the unstable region. For a sufficiently narrow jet, the dominant form of variability is a strengthening and weakening of the jet. On the other hand, for an extremely wide unstable region, two persistent jets emerge, both exhibiting zonal index characteristics. 5) During the major onset, the anomalously large eddy momentum flux convergence is typically associated with the merging of two PV fronts. In S. B. Feldstein and S. Lee (1996, manuscript submitted to *J. Atmos. Sci.*), two nearby troughs often combine to have a northeast–southwest tilt that leads to the initiation of a high-index state. In their case, one trough lies along the subtropical jet and the other along the midlatitude polar front jet. Therefore, although there is no subtropical jet in the two-layer QG model, perhaps one of the PV fronts in that model can be thought of as an analog of subtropical jet for the high index state. 6) Although composite energetics indicate that baroclinic growth is followed by barotropic decay during onset, both composite eddy heat flux and momentum flux convergence, and case studies suggest that a normal-mode baroclinic life cycle is unlikely to be relevant for either the onset or persistence of the zonal index. Notwithstanding that some of the necessary assumptions are questionable, explicit life cycle calculations also support the above conclusion. In particular, the outcome of the life cycle calculations are sensitive to the initial zonal winds that are chosen.

As discussed above, the persistence phase consists of a state of slow relaxation of the zonal flow, preceded by a single event of impulsive eddy forcing. This leads us to ask what determines the timescale of the persistence phase? In our model, both the thermal and frictional damping coefficients are expected to play a role. We would expect that the larger the value of these coefficients, the shorter the persistence timescale. In fact, in a series of preliminary calculations, it was found that as the surface friction coefficient was gradually increased, the zonal-flow anomaly decayed more rapidly. However, a more thorough exploration of parameter space is necessary to address this issue, as the results of Robinson (1996, manuscript submitted to *J. Atmos. Sci.*) suggest an opposite trend.

If a low-pass filter is applied to the impulsive eddy forcing, a different physical picture emerges. For example, Figs. 14a,b show sector model composites of low-pass (greater than 50 time units) vertically integrated zonal wind and eddy momentum flux convergence anomalies, respectively. These quantities should be compared with those from the unfiltered data shown in Figs. 8a,b. In addition to the smoothing of the anomalies, it can be seen that the filtering procedure has increased the persistence timescale for the momentum flux convergence anomaly to the extent that it is comparable to that of the zonal-wind anomaly. (Note that the persistence timescale for the zonal wind anomaly is essen-

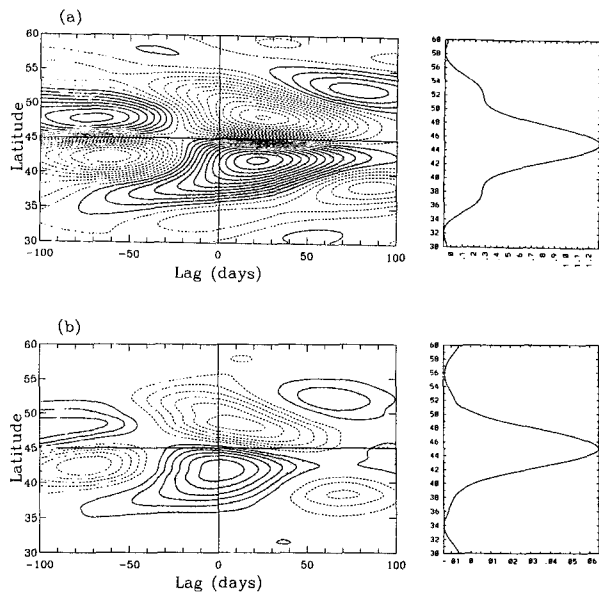


FIG. 14. Sector model composites of anomalous low-pass (a) barotropic zonal-mean zonal wind and (b) eddy momentum flux convergence. Contour intervals are (a)  $2 \times 10^{-2}$  and (b)  $2 \times 10^{-3}$ . Shading denotes values greater than or equal to the smallest positive contour level.

tially unaltered by the low-pass filter.) Thus, the implementation of this low-pass filter has in effect temporally smoothed the eddy forcing to the degree that this forcing no longer appears impulsive and instead gives the incorrect impression of a prolonged eddy–zonal-mean feedback.

The zonal-index behavior, as examined in this study, may be a model of the simplest form of low-frequency variability in the atmosphere. Most studies of atmospheric low-frequency variability concentrate on zonally asymmetric anomalies. These studies, which use highly filtered data, typically find contemporaneous symbiotic relationships between high- and low-frequency transient eddies. However, to the extent that the results of the present study are applicable to the more complex zonally asymmetric anomalies, a different picture would emerge. We examine these ideas by first equating the model's storm tracks with high-frequency transient eddies and the model's zonally averaged zonal wind with low-frequency transient eddies. Because the anomalous storm track follows the anomalous zonal-mean wind, this indicates that the former is forced by the latter. During this time period, despite the fact that the anomalous storm track is large, the anomalous zonal-mean wind is decaying because the eddy momentum flux convergence is negligible. On the other hand, during onset, even though the zonal-mean wind field is close to that of the climatological flow, the anomalous zonal-mean wind is forced impulsively by the storm

track eddies. Applying the analogies stated above, these results suggest that the mutual forcing of the high- (low-) frequency transient eddies by the low- (high-) frequency transient eddies occurs at different times, rather than a contemporaneous symbiotic relationship. Also, we emphasize that if the impulsive forcing of the low-frequency flow by high-frequency transient eddies occurs in the atmosphere, the persistence of low-frequency anomalies in the atmosphere may be simply characterized by a slow decay of the anomaly. However, the filtering and time-averaging techniques typically applied are not capable of diagnosing this behavior.

*Acknowledgments.* This research was supported by the National Science Foundation through Grant ATM-9416701. We wish to thank two anonymous reviewers for the beneficial comments that improved this manuscript.

#### REFERENCES

- Cai, M., 1992: An analytical study of the baroclinic adjustment in a quasigeostrophic two-layer channel model. *J. Atmos. Sci.*, **49**, 1594–1605.
- Chehelsky, P., and K. K. Tung, 1991: Nonlinear baroclinic adjustment. *J. Atmos. Sci.*, **48**, 1930–1947.
- Feldstein, S. B., and I. M. Held, 1989: Barotropic decay of baroclinic waves in a two-layer beta-plane model. *J. Atmos. Sci.*, **46**, 3416–3430.
- , and S. Lee, 1996: Mechanisms of zonal index variability in an aquaplanet GCM. *J. Atmos. Sci.*, in press.
- Horel, J. D., 1985: Persistence of the 500 mb height field during Northern Hemisphere winter. *Mon. Wea. Rev.*, **113**, 2030–2042.
- Hoskins, B. J., 1983: Modelling of the transient eddies and their feedback on the mean flow. *Large-Scale Dynamical Processes in the Atmosphere*. B. J. Hoskins and R. P. Pearce, Eds., Academic Press, 169–199.
- Karoly, D. J., 1990: The role of transient eddies in low-frequency zonal variations of the Southern Hemisphere. *Tellus*, **42A**, 41–50.
- Kidson, J. W., 1988: Indices of the Southern Hemisphere zonal wind. *J. Climate*, **1**, 183–194.
- Lee, S., and I. M. Held, 1991: Subcritical instability and hysteresis in a two-layer model. *J. Atmos. Sci.*, **48**, 1071–1077.
- Mo, K. C., 1986: Quasi-stationary states in the Southern Hemisphere. *Mon. Wea. Rev.*, **114**, 808–823.
- Nigam, S., 1990: On the structure of variability of the observed tropospheric and stratospheric zonal-mean zonal wind. *J. Atmos. Sci.*, **47**, 1799–1813.
- Panetta, R. L., 1993: Zonal jets in wide baroclinically unstable regions: Persistence and scale selection. *J. Atmos. Sci.*, **50**, 2073–2106.
- , and I. M. Held, 1988: Baroclinic eddy fluxes in a one-dimensional model of quasigeostrophic turbulence. *J. Atmos. Sci.*, **45**, 3354–3365.
- Robinson, W., 1991: The dynamics of the zonal index in a simple model of the atmosphere. *Tellus*, **43A**, 295–305.
- , 1996: Does eddy feedback sustain variability in the zonal index? *J. Atmos. Sci.*, in press.
- , and J. Qin, 1992: Predictability of the zonal index in a global model. *Tellus*, **44A**, 331–338.
- Rossby, C. G., 1939: Relations between variations in the intensity of the zonal circulation and the displacements of the semi-permanent centers of action. *J. Mar. Res.*, **2**, 38–55.

- Simmons, A. J., and B. J. Hoskins, 1978: The life cycles of some nonlinear baroclinic waves. *J. Atmos. Sci.*, **35**, 414–432.
- Treguier, A. M., and R. L. Panetta, 1994: Multiple zonal jets in a quasigeostrophic model of the Antarctic Circumpolar Current. *J. Phys. Oceanogr.*, **24**, 2263–2277.
- Trenberth, K. E., 1979: Interannual variability of the 500 mb zonal mean flow in the Southern Hemisphere. *Mon. Wea. Rev.*, **107**, 1515–1524.
- , 1984: Interannual variability of the Southern Hemisphere circulation: Representativeness of the year of the Global Weather Experiments. *Mon. Wea. Rev.*, **112**, 108–123.
- Willett, H. C., 1948: Patterns of world weather changes. *Eos, Trans. Amer. Geophys. Union*, **29**, 803–809.
- Yu, J. Y., and D. L. Hartmann, 1993: Zonal flow vacillation and eddy forcing in a simple GCM of the atmosphere. *J. Atmos. Sci.*, **50**, 3244–3259.